

## STUDYING THE SMALL-SCALE STRUCTURE OF A POLARIZATION JET DURING THE APRIL 20, 2018 GEOMAGNETIC STORM

**A.A. Sinevich**

Space Research Institute of RAS,  
Moscow, Russia, sinevich.aa@gmail.com  
National Research University Higher School of Economics,  
Moscow, Russia, sinevich.aa@gmail.com

**A.A. Chernyshov**

Space Research Institute of RAS,  
Moscow, Russia, achernyshov@iki.rssi.ru

**D.V. Chugunin**

Space Research Institute of RAS,  
Moscow, Russia, dimokch@mail.ru

**W.J. Miloch**

Department of Physics, University of Oslo,  
Oslo, Norway, w.j.miloch@fys.uio.no

**M.M. Mogilevsky**

Space Research Institute of RAS,  
Moscow, Russia, mogilevsky2012@gmail.com

---

**Abstract.** In this work, we study the small-scale structure of a polarization jet in the subauroral region during the April 20, 2018 geomagnetic storm. We report measurement results of plasma parameters inside the polarization jet with a maximum sampling rate of up to 1 kHz, obtained with Langmuir probes installed on the NorSat-1 microsatellite. The study establishes the presence of temperature and electron density inhomogeneities inside the polarization jet with spatial dimensions of

tens to hundreds of meters. The previously known features of the polarization jet evolution have been confirmed. We have also found that the distribution of the electron temperature inside the jet forms two separate peaks as the geomagnetic activity develops during the storm.

**Keywords:** polarization jet, subauroral ionosphere, geomagnetic activity, satellite data.

---

### INTRODUCTION

The subauroral ionosphere is a region of Earth's ionosphere at geomagnetic latitudes from  $50^{\circ}$ – $55^{\circ}$  to  $65^{\circ}$ – $70^{\circ}$ , which is located between the projections along geomagnetic field lines of the plasmapause and equatorial boundary of the auroral oval. In other words, the subauroral ionosphere is a transition region between the mid-latitude and high-latitude ionosphere. Its position changes rapidly during geomagnetic activity. In this ionospheric region there are physical processes and phenomena that are absent or less pronounced at other latitudes such as formation of the main ionospheric trough (MIT) in the latitudinal distribution of the plasma electron density [Stepanov et al., 2017]; formation of the trough polar wall due to precipitation of low-energy electrons at the equatorial boundary of diffuse invasions [Bryunelli, Namgaladze, 1988]; formation of a trough of light ions in the upper ionosphere [Galperin et al., 1990]; radio aurora [Kotova et al., 2020]; appearance of red arcs in the background airglow [Ivenko et al., 2001]; strong thermal emission velocity enhancement (STEVE) [MacDonald et al., 2018]. This region also exhibits narrow streams of fast westward subauroral ion drifts near the plasmapause projection at heights of the ionospheric F layer, which are most pronounced during magnetic storms/substorms against the background of large-scale plasma convection [Foster et al., 1978; Anderson et al., 1991]. Such streams were first recorded by the Soviet satellite Cosmos-184 and were called “polarization jet” (PJ) [Galperin et al., 1973a, b; Galperin et al., 1974]. In English literature after the work [Spiro et al., 1979], in which the narrow streams of ion drifts were examined using data from the American satellite Atmosphere Explorer C, this phenomenon was termed “subauroral ion drift” (SAID). At ionospheric heights, the polarization

jet bandwidth in latitude is  $1^{\circ}$ – $2^{\circ}$ , and the drift velocity is from  $\sim 1$  km/s or higher in a westerly direction, as recorded in the dusk and night sectors of the local magnetic time (MLT). At the same time, in the dusk sector ( $< 20$  MLT) there are wide ion flows [Karlsson et al., 1998; Figueiredo et al., 2004]. Foster and Burke [2002] have combined these two types of observed subauroral ion drifts: narrow ion drift jets (PJ) and wide ionospheric convection regions to the west with high velocities, as well as their associated electric fields, aka subauroral polarization stream (SAPS), thereby suggesting that they have the same formation mechanisms. These phenomena (SAPS and PJ) have been observed and investigated using both satellite data and ground measurements from a chain of ionospheric stations and incoherent scatter radars [Anderson et al., 1991, 1993, 2001; Foster, Vo, 2002; Galperin, 2002; Bondar et al., 2005; Koustov et al., 2006; Stepanov et al., 2011, 2017, 2019a, b; Khalipov et al., 2016a, b, etc.]. A drop in the ionospheric plasma density in the F layer inside a polarization jet significantly affects short-wavelength radio emission propagation conditions, which indicates the practical importance in studying PJ.

Despite the importance of using a variety of ground-based observation tools for studying and analyzing PJ and SAPS signatures, as well as for working out analytical models and numerical simulation, of the highest value are the direct measurements that can be made only when a satellite passes through the subauroral region during PJ/SAPS development. As noted above, PJ were discovered due to satellites Cosmos-184 and Atmosphere Explorer C [Galperin et al., 1973a, b; Galperin et al., 1974; Spiro et al., 1979]. Subsequently, the satellite data was extensively used for determining properties and structures of PJ and SAPS. Based on observations

made during many space missions, mechanisms that drive PJ/SAPS have been proposed and distinctive features of their behavior during geomagnetic storms and substorms have been found. For example, satellite data was used from OGO-6 [Maynard, 1978] Oreol-1 and -2 [Khalipov et al., 1977; Galperin et al., 1977], ICEE-1 [Maynard et al., 1983] Oreol-3 [Benkova et al., 1985], DE-1 and DE-2 [Anderson et al., 1993], CRESS [Rowland, Wygant, 1998; Burke et al., 1998], Freja [Karlsson et al., 1998], Astrid-2 [Figueiredo et al., 2004], AMPT/CCE [Khalipov et al., 2003], DEMETER [Seran et al., 2008], Cluster, THEMIS, and Van Allen Probes (RBSP) [Mishin et al., 2017]. A large number of works on PJ and SAPS were carried out using DMSP satellite data. The DMSP data supported the statistical analysis of PJ and SAPS characteristics, along with data from incoherent scatter radars and from a chain of ionospheric stations, which was acquired when DMSP satellites crossed the subauroral polarization stream. Moreover, the DMSP observations were compared with the results obtained from other satellites (e.g., [Anderson et al., 2001; Foster, Burke, 2002; Foster, Vo, 2002; Mishin et al., 2010; Wang et al., 2012; Mishin, 2013; He et al., 2014; Khalipov et al., 2016a, b] etc.).

Complex studies involving a variety of space missions have revealed basic large-scale features of the formation and evolution of PJ and SAPS, have determined the place where subauroral ion drifts are most likely to occur, and time of their occurrence, as well as have established their relationship with geomagnetic disturbances. However, many satellites were not equipped with necessary instrumentation for studying in more detail characteristics of electromagnetic and plasma disturbances observed in the outer ionosphere when the satellites were flying over subauroral latitudes during PJ; or the on-board instruments could not make high temporal resolution measurements. Small-scale processes in PJ/SAPS are poorly studied, and many questions remain to be answered. In this paper, we use data from the microsatellite NorSat-1, which measured ionospheric plasma parameters in situ with Langmuir probes at a maximum sampling rate of 1 kHz (by comparison, plasma density measurements made by the DMSP satellite are available with a sampling rate of 1 Hz). This allows us to study the PJ small-scale structure in the subauroral region during geomagnetic activity, which is the main purpose of our work.

## CALCULATION OF IONOSPHERIC PLASMA PARAMETERS

The Norwegian microsatellite NorSat-1 (~16 kg, 23×39×44 cm) was launched on July 14, 2017 from the cosmodrome of Baikonur into a circular sun-synchronous orbit with an inclination of 98°, a height of ~600 km, and an orbital period of 95 min. Its primary task is to identify vessels in Norwegian waters, using the Automatic Identification System (AIS). In addition, the satellite is equipped with two scientific instruments: Compact Lightweight Absolute Radiometer (CLARA) for monitoring the solar radiation and the multi-Needle Langmuir Probe (m-NLP) developed by the University of Oslo [Hoang et al., 2018].

As is known, the classical Langmuir probe makes measurements at a voltage range and provides a current-voltage characteristic, which is used to calculate plasma parameters. Since it takes time to cover the full range, temporal resolution of resulting plasma parameters is generally low, thus impeding the study of small-scale plasma structures. The multi-needle system of Langmuir probes installed in the NorSat-1 microsatellite consists of four cylindrical probes (needles) at different voltage bias within the electron saturation region of the current-voltage characteristic [Hoang et al., 2018].

Absence of sweeping across the probe voltage bias enables us to measure the electron current much more frequently, and thereby to obtain high-frequency plasma characteristics. The electron saturation current of a cylindrical probe with a radius much smaller than the Debye radius is given by the Orbital Motion Limited (OML) theory, whose fundamentals were developed by Mott-Smith and Langmuir [Mott-Smith, Langmuir, 1926]. To determine the electron density  $N_e$  in measurements by the system of Langmuir probes, at least two cylindrical probes operating at different fixed voltages are used [Jacobsen et al., 2010]:

$$N_e = \frac{1}{KA} \sqrt{\frac{\Delta(I_c)^2}{\Delta V_b}}, \quad (1)$$

where  $K$  is the constant equal to  $\frac{e^{3/2}}{\pi} \sqrt{\frac{2}{m_e}}$ ;  $\Delta(I_c)^2$  is the difference of squared collected currents;  $A$  is the surface area of the probe;  $\Delta V_b$  is the probe voltage difference.

A key feature of m-NLP is that it does not need information about plasma potential and electron temperature to measure the electron density. The electron temperature in eV is calculated from the following formula:

$$T_e = \frac{R(V_s + V_{p2}) - (V_s + V_{p1})}{1 - R}, \quad (2)$$

where  $V_s$  is the satellite potential;  $V_{p1}$  and  $V_{p2}$  are the fixed potentials of probes;  $R = \frac{I_{c1}^2}{I_{c2}^2}$ ; where  $I_{c1}$  and  $I_{c2}$  are the currents measured by probes, which are at potentials  $V_{p1}$  and  $V_{p2}$  respectively.

Since we do not know the satellite potential, we cannot calculate accurate temperature values from this formula for the region of electron saturation of the current-voltage characteristic of the Langmuir probes. However, while the absolute electron temperature cannot be derived without knowing the satellite potential in accordance with the Langmuir probe theory, we can calculate the absolute temperature variation and thus study the temperature variation with time and latitude.  $T_e$  does not therefore refer only to temperature further in the text.

## MEASUREMENT RESULTS AND THEIR ANALYSIS

We examine the storm that occurred on April 20, 2018. Figure 1 presents the geomagnetic indices *SME*

(a) [Newell, Gjerloev, 2011] and  $Dst$  (b) [Nose et al., 2015] that characterize geophysical conditions on April 20 and April 19–21, 2018 respectively. For clarity, red arrows in Figure 1, a, b show the time of the satellite passes considered below. X-axes in Figure 1, a, b have different duration so that we can see all storm phases in Figure 1, b (plot of the  $Dst$  index). The smaller time interval of the X-axis in Figure 1, a is selected to better illustrate a change in the  $SME$  index between NorSat-1 passes. A moderate geomagnetic storm began after 02 UT. As it follows from Figure 1, a, the maximum value of the  $SME$  index, which describes the auroral electrojet, was observed at about 10 UT and was more than 1500 nT. As seen in Figure 1, b, about 10 UT on April 20 the geomagnetic storm recovery phase began, and at the same time auroral geomagnetic activity (Figure 1, a) was the highest. Thus, on April 20, 2018 the probability of finding a polarization jet was the highest [Anderson et al., 1993; Foster, Vo, 2002].

Figure 2 shows trajectories of the NorSat-1 passes

described below. Along the angular axis is the local magnetic time; along the radial axis are invariant latitudes. Crosses in Figure 2 mark the middle of PJ during each satellite pass. Since the satellite orbit is circular sun-synchronous, its height above the Earth surface was virtually unchanged in the time interval of interest ( $\sim 600$  km).

The processed measurements made by Langmuir probes in the subauroral ionosphere during the NorSat-1 pass from the northern polar cap to the equator at a height of  $\sim 600$  km are presented in Figure 3. Figure 3 depicts the electron density and temperature values calculated by the method described in the previous section. Since the measurements were performed with a nominal sampling rate of  $\sim 1$  kHz, the plots show values averaged over 100 points, i.e. the moving average procedure was applied to data processing. Figure 3 presents measurements made from 10:10:10 to 10:13:00 UT when the satellite was in the Northern Hemisphere in the near-midnight sector ( $\sim 01$  MLT) and the  $SME$  index was maximum.

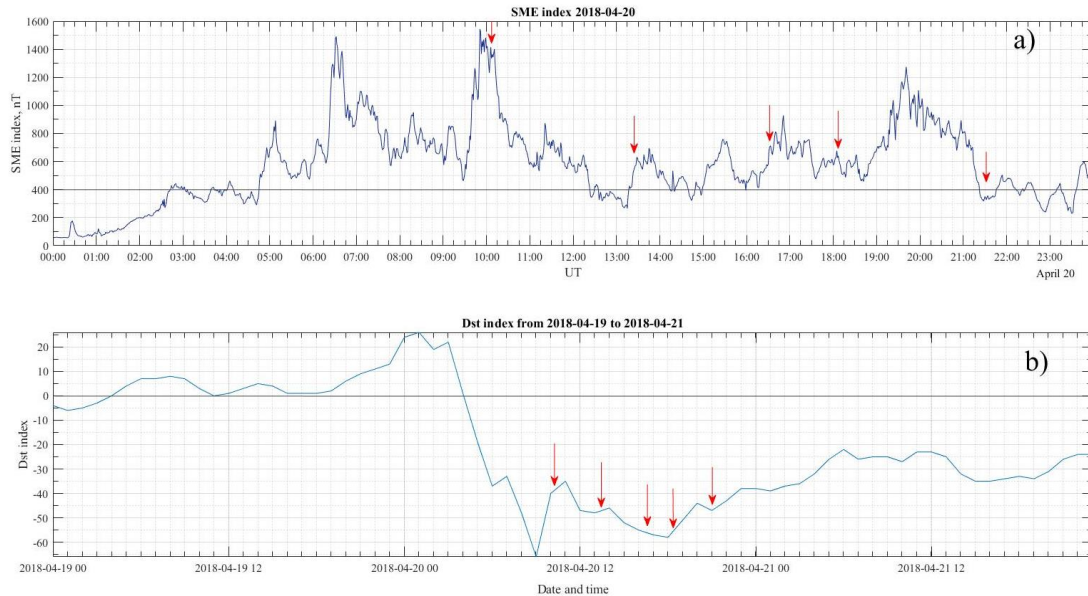


Figure 1.  $SME$  on April 20, 2018 (a) and  $Dst$  on April 19–22, 2018 (b). Red arrows indicate the time of the satellite passes considered below (10, 13, 16, 18, and 21 UT); the gray line shows levels of 400 nT (a) and 0  $Dst$  (b)

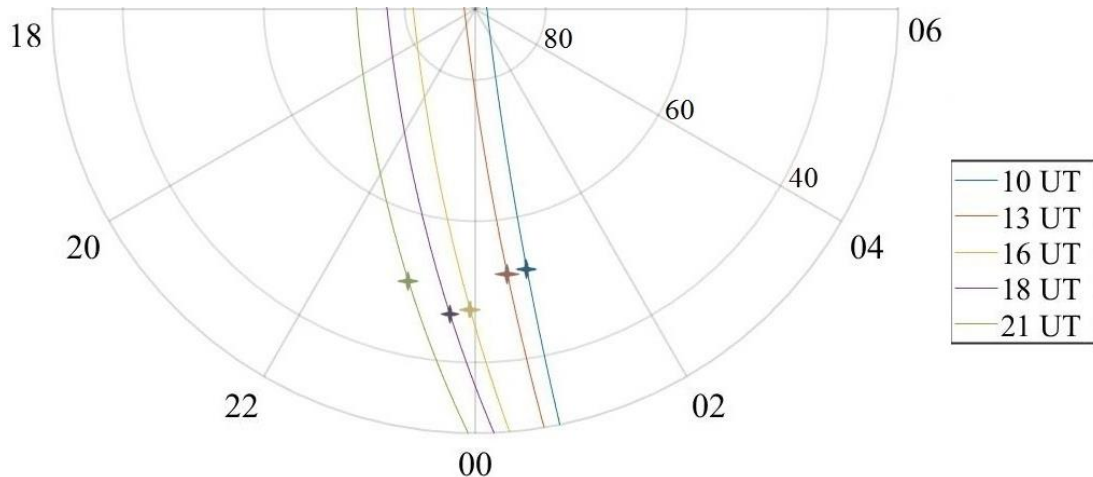


Figure 2. NorSat-1 trajectories on April 20, 2018 at 10, 13, 16, 18, and 21 UT in polar coordinates. The angular axis represents MLT; the radial axis, invariant latitudes; crosses mark PJ locations on the satellite trajectories



Figure 3. Temperature and electron density variations during the NorSat-1 pass at 10:10:10–10:13:00 UT on April 20, 2018. The red arrow shows the polarization jet location; black vertical lines denote the time when the satellite crossed L-shells 4 and 3

The left Y-axis shows the electron density values (blue curve); the right one, the electron temperatures (red curve), the bottom horizontal axis indicates the measurement time (UT); the top one, the invariant latitude of the satellite. Vertical black lines denote the times when the satellite crossed L-shells.

From the orbital data it follows that during that period the satellite was at subauroral and plasmaspheric latitudes. It is impossible to identify exact location of the subauroral ionosphere boundaries only from the electron density measurements — this requires simultaneous measurements of energetic electron and proton precipitation. Nonetheless, relying on many previous studies of PJ we can indirectly estimate boundaries in the inner magnetosphere and find out when the satellite passed through the polarization jet. As is known from various papers (e.g., [Galperin, 2002]), PJ is located inside the main ionospheric trough and is often situated on its polar wall, at the boundary of diffuse electron precipitation (soft electron boundary, SEB). Figure 3 indicates that at 10:11:25 there was a rapid decrease in electron density, and then till 10:12:04 the plasma density gradually recovered. We can confidently assert that the satellite that time crossed MIT, whose minimum was at the invariant latitude of  $\sim 53^\circ$ .

More poleward of MIT (Figure 3), the electron density is higher than the background level  $\sim 2$  times due to charged particle precipitation from the magnetosphere. Thus, we can say that PJ should be located on the polar wall of MIT. Indeed, looking at the electron temperature values shows that in the region more poleward of MIT the temperature is higher due to electron precipitation, but at the polar boundary of MIT we can also see a slight temperature rise. This time instance is indicated in Figure 3 by the red arrow.

Figure 4 presents more detailed measurements during this pass. We can see that at the MIT polar boundary there is a local electron density trough, which is accompanied by an about 1.5-fold increase in the electron temperature. This time instance is shown by the red arrow (top panel). Such behavior of the electron density and temperature, as well as the location of the trough suggest that the satellite crossed the PJ that time. The

polarization jet was recorded at 10:11:25–10:11:30 UT; its approximate boundaries (indicated by green lines in this and subsequent figures) were at invariant latitudes from  $53.37^\circ$  to  $53.22^\circ$ . Thus, the spatial scale of PJ in latitude was  $\sim 0.15^\circ$ , which at 600 km above the Earth surface corresponds to a width of 18 km. Furthermore, as it follows from the temperature and electron density plots (top panel), besides the narrow PJ structure on the polar edge of MIT we can see several regions with a temperature higher than the background level, which coincide with a small electron density decrease. This suggests that MIT contains several narrow structures more equatorward of PJ. Since PJ is accompanied by a strong meridional drift with a velocity exceeding the velocity of sound; small-scale plasma irregularities caused by various instabilities such as the Farley-Buneman instability are expected to develop within it. To detect them, on the middle and bottom panels of Figure 4 we present temperature and electron density spectrograms respectively, obtained through the discrete Fourier transform of unaveraged satellite data. The spectrograms show an increase in the electron temperature spectral intensity at frequencies up to  $\sim 300$  Hz and in the electron density spectral intensity at frequencies up to  $\sim 100$  Hz. Note that the density spectral intensity peak appears  $\sim 1$  s before the temperature peak. This effect is most likely caused by the Fourier processing of the steep drop in the electron density. From these spectrograms we can infer that there are small-scale temperature irregularities in PJ with spatial scales of tens to hundreds of meters.

Moreover, in Figure 4 more equatorward of the polarization jet there is a region bounded by a slight electron density increase on the equatorward side (blue arrow) at the invariant latitude of  $52.2^\circ$  (10:11:44 UT). In this region there are several areas with appreciable,  $\sim 1.2$ -fold electron density increases, and respective spectral intensity increases at frequencies to  $\sim 250$  Hz (middle panel). From the foregoing observations and on the assumption that the polar boundary of this region coincides with the polar boundary of PJ, we can hypothesize that this region is a broad westward SAPS inside which the polarization jet is usually located [Foster,

Burke, 2002]. Figure 5 depicts a satellite pass at 13 UT in the 01 MLT near-midnight sector. The polarization jet was observed at 13:22:56–13:23:21 UT at the  $53.3^{\circ}$ – $51.74^{\circ}$  invariant latitude. We can see (top panel) that within three hours after the first pass (10 UT) the polarization jet expanded toward the equator, and its width became  $\sim 1.54^{\circ}$ , i.e.  $\sim 188$  km. Nonetheless, its polar boundary remained at approximately the same latitude —  $\sim 53.3^{\circ}$ . The electron density trough in PJ became more pronounced and deeper: we can see its polar boundary from the  $\sim 1.5$ -fold electron density decrease compared to the background level in MIT for 1–2 s. The equatorward boundary of PJ is less pronounced, the electron density when crossed grows for  $\sim 10$  s, with the electron density inside PJ and outside of the equatorward boundary differing  $\sim 2$  times. This suggests that the PJ equatorward boundary coincides with the MIT boundary. Thus, we can say that for three hours after its occurrence, the polarization jet

moved from the polar wall of the main ionospheric trough to its equatorward wall. In addition, Figure 5 indicates that the electron temperature distribution peak in PJ has shifted from the center closer to the equatorward boundary and is now located at the invariant latitude of  $52.3^{\circ}$  ( $\sim 13:23:13$  UT). The electron density and temperature spectrograms in the middle and bottom panels of Figure 5 respectively suggest that compared to the satellite pass at 10 UT the spectral intensity at high frequencies decreased  $\sim 2$  times. This can be explained by the fact that on April 20, 2018 at 13 UT auroral geomagnetic activity was the lowest (Figure 1, a): the SME index was  $\sim 250$  nT. Moreover, in the spectrogram the electron temperature intensity increase inside PJ relative to the background is located from the PJ polar wall at the invariant latitude of  $53.3^{\circ}$  to the temperature distribution peak at the invariant latitude of  $52.3^{\circ}$ .

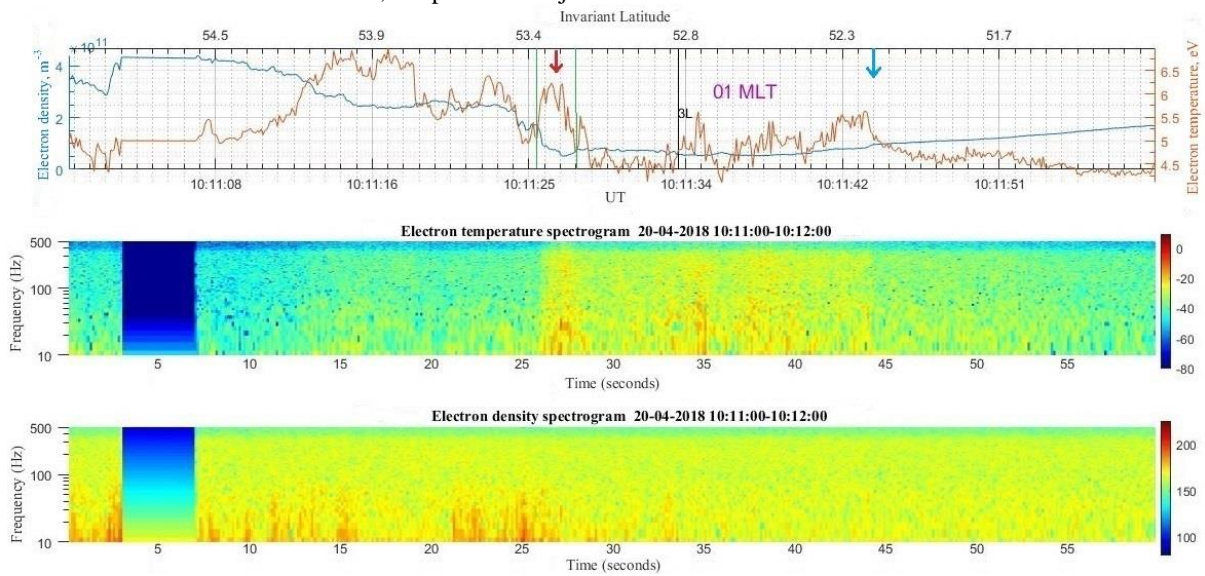


Figure 4. Electron density and temperature variations during the passage at 10 UT and their spectrograms. The red arrow indicates the polarization jet; vertical green lines mark approximate boundaries of the polarization jet; the vertical black line is the time when the satellite crossed L-shell 3; the blue arrow shows the estimated equatorial boundary of the westward SAPS

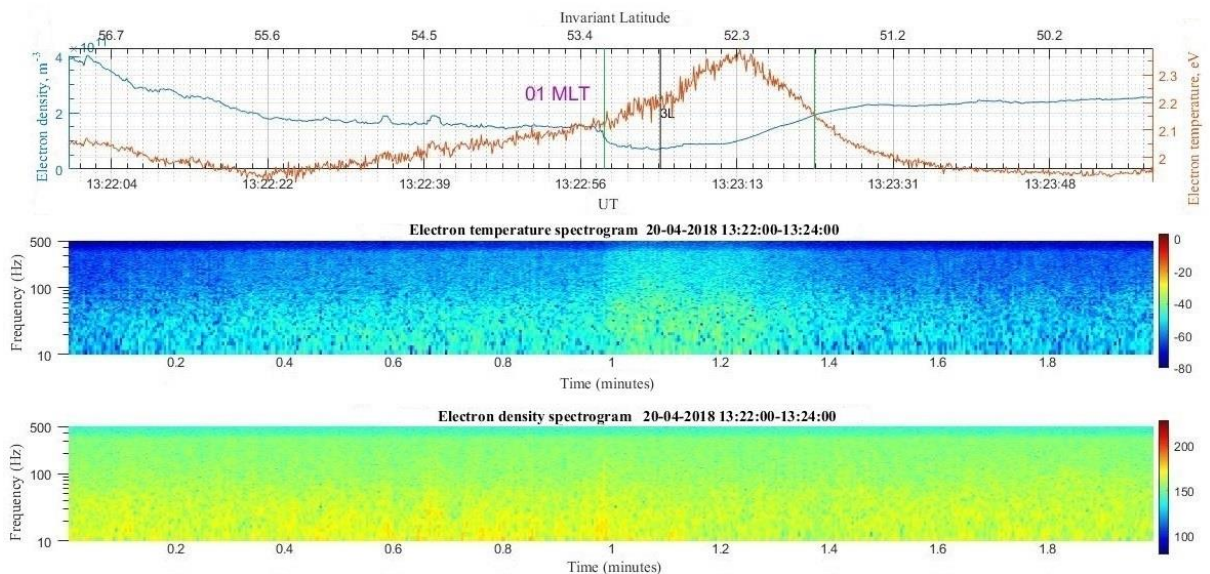


Figure 5. Electron density and temperature variations during the passage at 13 UT and their spectrograms. Vertical green lines indicate approximate boundaries of the polarization jet; the vertical black line is the time when the satellite crossed L-shell 3

Figure 6 illustrates a satellite pass at 16 UT in the 0 MLT sector. According to Figure 6, by the time of this pass the polarization jet expanded in latitude to  $\sim 1.7^\circ$ , which corresponds to  $\sim 207$  km, its approximate boundaries in the time interval 16:36:46–16:37:16 UT were at invariant latitudes from  $48.3^\circ$  to  $46.8^\circ$ . It is noticeable that three hours after the previous pass PJ shifted to the equator by  $\sim 5^\circ$ . As inferred from Figure 6, the polar boundary of the polarization jet located at the invariant latitude of  $48.3^\circ$  (16:36:46 UT) is characterized by a drop in the electron density relative to its average value in MIT 2–3 times for  $\sim 1.5$  s. It is worth noting that the plot of the electron density in PJ is almost a straight line. This means that the electron density during the pass at 16 UT inside PJ was constant across its width. At the equatorward boundary of the polarization jet located at an invariant latitude of  $\sim 46.8^\circ$  (16:37:16 UT), the electron density increased 4–5 times for  $\sim 9$  s. This implies that the PJ location relative to MIT has not changed: its equatorward wall still coincides with the equatorward wall of the main ionospheric trough. The electron density drops much more rapid and more pronounced than during previous NorSat-1 passes and other satellite measurements with a lower sampling rate at PJ boundaries allow us at time scales of 1 ms to confirm that the polarization jet coincides with the electron density trough inside MIT. As clearly seen in Figure 6, inside PJ at a distance of  $\sim 0.8^\circ$  two electron temperature distribution peaks appeared. The first peak, located closer to the poleward edge of PJ, is at the  $48.15^\circ$  invariant latitude (16:36:55 UT) and exhibits an about 1.42-fold increase in the electron temperature relative to the background. The second, more equatorward peak, located at the  $47.55^\circ$  invariant latitude (16:37:05 UT), corresponds to an about 1.66-fold temperature rise. Thus, the equatorial peak is more intense than the polar one. Moreover, the electron temperature spectrogram (middle panel) also

shows two respective peaks, an increase of the spectral intensity of which is more pronounced as compared to the previous pass and reaches frequencies of  $\sim 300$  Hz. The formation of separate electron temperature distribution peaks inside the polarization jet, with irregularities having spatial scales of tens to hundreds of meters, can be both a new effect first discovered in this work and the beginning of the formation of a double-peak structure of the polarization jet (double-peak subauroral ion drifts, DSAID). DSAID are described by He et al. [2016]; the authors have performed a statistical analysis of DMSP data.

Figure 7 illustrates a satellite pass at 18 UT in the 0 MLT sector. The polarization jet is at invariant latitudes from  $47.2^\circ$  to  $\sim 45.9^\circ$  (from 18:13:58 to  $\sim 18:14:20$  UT). The equatorward boundary of PJ, which during previous passes was less pronounced than the poleward one, dramatically expanded during this pass, so its location and the PJ width were determined with great inaccuracy. As shown in Figures 6 and 7, after having expanded to the maximum size during the pass at 16 UT, the PJ began to narrow as geomagnetic activity decreased, and by the pass at 18 UT its width was  $\sim 1.3^\circ$ , or  $\sim 159$  km. In this case, it is noticeable that PJ moved by  $\sim 1.5^\circ$  of invariant latitude closer to the equator than during the pass at 16 UT. We can see that in the electron temperature distribution inside PJ the two peaks were transformed into two separate regions. The first region at 18:13:58–18:14:05 UT is located at invariant latitudes from  $47.35^\circ$  to  $46.85^\circ$ , the electron temperature therein is on average  $\sim 1.37$  times above the background level. The second region is at the invariant latitude of  $46.4^\circ$  to  $46.75^\circ$  (18:14:07–18:14:20 UT) and exhibits an about 1.5-fold electron temperature increase compared to the background level. Thus, the equatorward region, as during

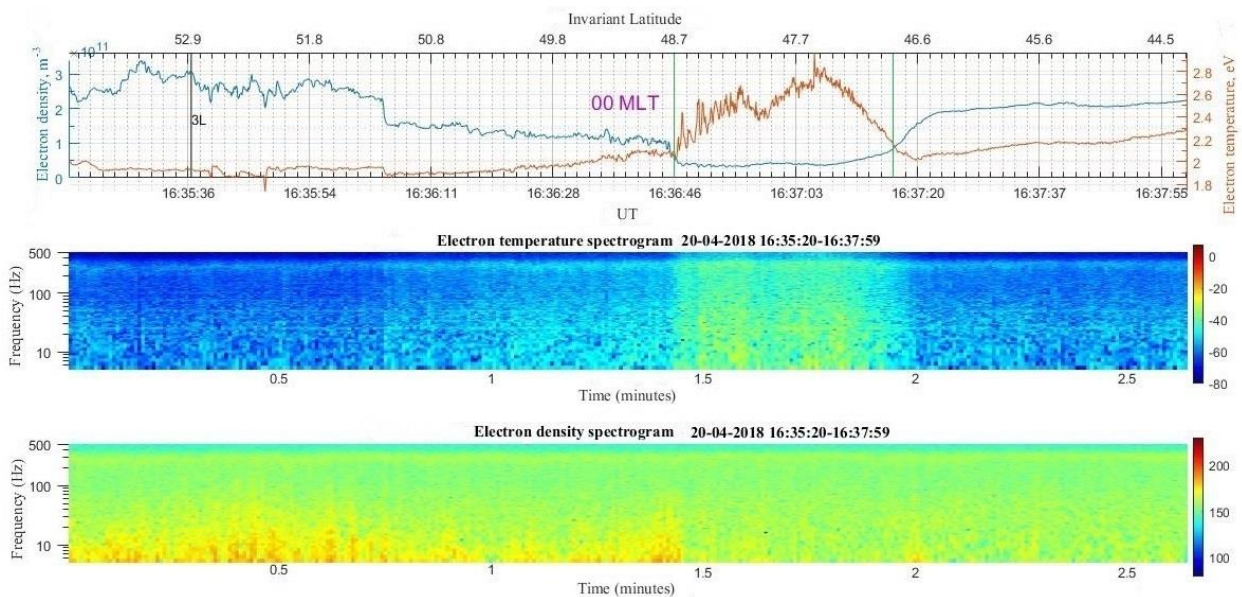


Figure 6. Electron density and temperature variations during the pass at 16 UT and their spectrograms. Vertical green lines are approximate boundaries of the polarization jet; the vertical black line is the time when the satellite crossed L-shell 3

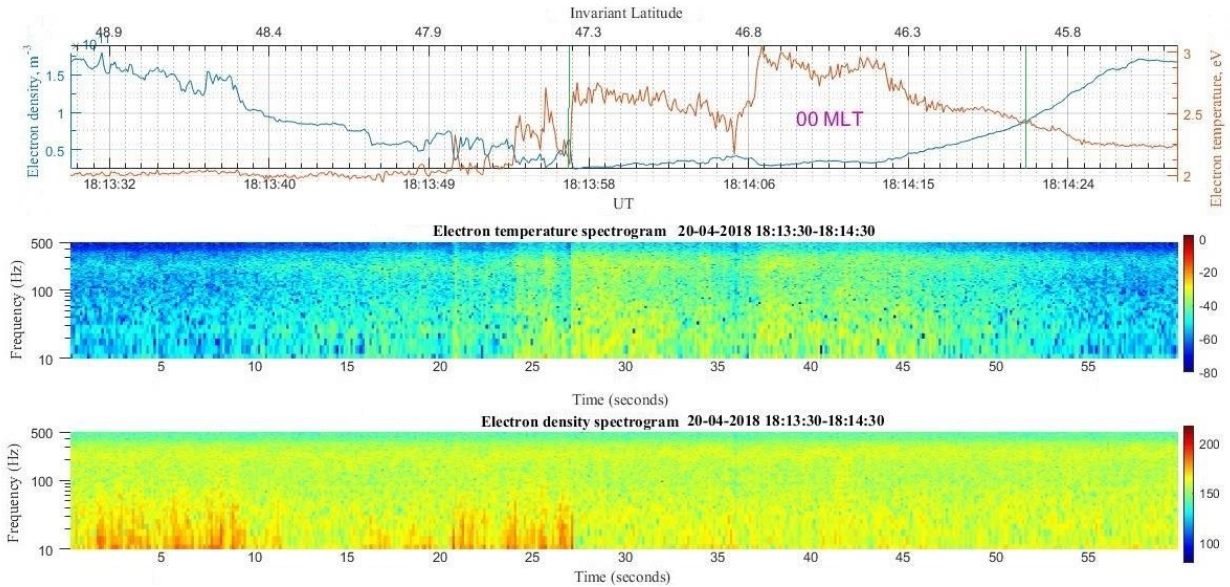


Figure 7. Electron density and temperature variations during the pass at 18 UT and their spectrograms. Vertical green lines are approximate boundaries of the polarization jet

the pass at 16 UT, is more intense than the poleward one. Figure 7 shows that to each of the regions with increased electron temperature corresponds a small trough in the electron density distribution. The electron temperature spectrogram (Figure 7, middle panel) also displays two regions. These observations suggest that at the time of the pass at 18 UT one polarization jet split into two jets and this event was preceded by two separate temperature peaks identified during the pass at 16 UT.

Figure 7 also indicates that more poleward of the polarization jet there are two small electron temperature peaks at the invariant latitudes of  $\sim 47.5^\circ$  and  $\sim 47.6^\circ$ , the equatorward peak being by  $\sim 5\%$  more intense than the poleward one. Existence of these peaks can be explained both by a random effect in the complicated structure of the ionosphere in the subauroral region and by the fact that these peaks are remains of the double-peak PJ, whose formation during the pass at 16 UT is illustrated in Figure 6. If the latter is true, we can confidently assert that the polarization jet, indicated by green lines in Figure 7, was not produced by the PJ recorded during the pass at 16 UT — it is a new PJ driven by increasing geomagnetic activity at 17 UT (Figure 1, *a*). As follows from Figure 8, which shows the satellite pass at 21 UT in the 0 MLT sector, the polarization jet in the time interval from 21:27:17 to  $\sim 21:27:30$  UT is at invariant latitudes from  $52.15^\circ$  to  $\sim 51.4^\circ$ .

The equatorward boundary of the polarization jet during this pass is less pronounced than during the pass at 18 UT. This means that its location and PJ width during the pass at 21 UT have been identified with a great inaccuracy. According to Figures 8, 7, and 1 *b*, three hours later the pass at 18 UT when geomagnetic activity went down the polarization jet narrowed to  $\sim 0.75^\circ$ , or  $\sim 91$  km, and moved in latitude by  $\sim 5^\circ$  poleward. The electron density trough became smoother and almost merged with MIT. Figure 8 also indicates that the two regions of electron temperature

distribution coalesced into a single structure whose temperature differed from the background level  $\sim 1.5$  times. The electron temperature spectrogram (Figure 8, middle panel) displays spectral intensity increases to 300–400 Hz, and four lines, in three of which the spectral intensity is high at all frequencies up to  $\sim 500$  Hz: at 21:27:17, 21:27:19, and 21:27:23 UT at invariant latitudes of  $52.15^\circ$ ,  $52^\circ$ , and  $51.82^\circ$ . The fourth, less pronounced line whose spectral intensity is high at frequencies to 100–200 Hz is located at the invariant latitude of  $51.7^\circ$  (21:27:25 UT). Note that location of the first line coincides with the assumed poleward boundary of the polarization jet.

In Figure 8, more poleward of the polarization jet at the invariant latitude of  $52.2^\circ$  there is a small peak in the electron temperature. If the assumption that the two small peaks poleward of PJ in Figure 7 are remnants of PJ [Anderson et al., 1991] observed during the pass at 16 UT (Figure 6), is true, the peak in Figure 8 might have arisen from the coalescence of these two structures. We can also suspect that this peak is remnants of two areas of the PJ observed during the pass at 18 UT (Figure 7), which merged into a single structure. In this case, PJ in Figure 8 is new, arising presumably during the considerable (1200 nT) increase in geomagnetic activity at 20 UT, which can be seen in Figure 1, *a*. On the other hand, due to the fact that the previous PJ was located at lower latitudes, as geomagnetic activity goes down the magnetospheric convection and energetic particle precipitation boundaries shift a few degrees more poleward, with PJ remaining more equatorward and eventually disappearing during relaxation. Perhaps that is why during the pass at 21 UT a new PJ structure, which appeared more poleward of the preceding PJ, is observed. These issues require further study.

Note that from DMSP data the cases have been found when during one satellite pass two peaks of PJ velocities were seen, i.e. the so-called double-peak subauroral ion drift (DSAID) [He et al., 2016].

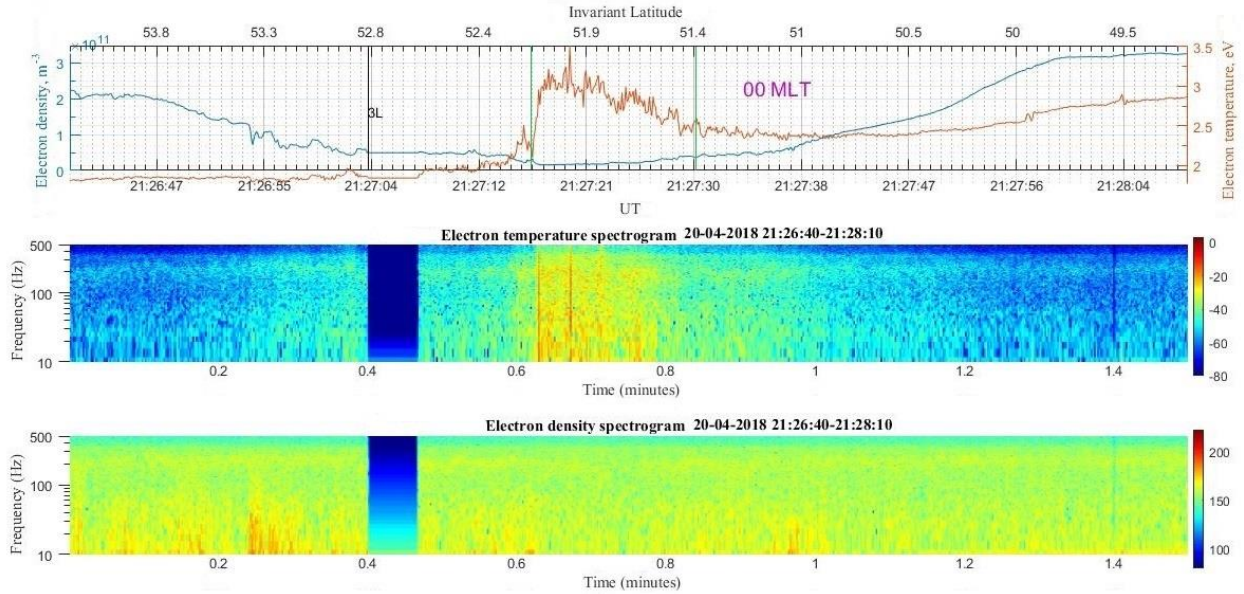


Figure 8. Electron density and temperature variations during the pass at 21 UT and their spectrograms. Vertical green lines are approximate boundaries of the polarization jet; the vertical black line is the time when the satellite crossed L-shell 3

These results were later confirmed by Wei et al. [2019], using not only DMSP measurements, but also those from Van Allen Probes (RBSP). It is useful to compare the splitting of electron temperature and density into the two areas, shown in Figures 6, 7, and 8, with DSAID. According to [He et al., 2016], DSAID has the following features:

1. In 90 % of DSAID, a single polarization jet first appears in the dusk–midnight MLT sector. Then, its temperature and drift velocity peak splits into two in the sectors before 20 MLT and after 21 MLT. During the recovery phase of the geomagnetic event, the peaks may disappear or merge first into one peak and then disappear at the end of the geomagnetic storm recovery phase. In the rest 10 % of cases, two small peaks arise simultaneously which, depending on MLT, eventually either merge, becoming a strong double-peak PJ, or coalesce into one strong polarization jet.

2. As MLT increases relative to 21 MLT, the equatorward peak decreases, whereas the poleward one increases.

3. DSAID occurs usually during higher geomagnetic activity than the ordinary PJ.

In this study, we note the following:

1. At 00 MLT there is a polarization jet with two peaks of electron temperature distribution inside (16 UT), which then splits into two distribution regions (18 UT). As the magnetic storm recovery phase develops, these two regions decrease and merge into one peak (21 UT).

2. For the 00 MLT sector, Figures 6 and 7 show that the equatorward peak is higher than the poleward one, compared to DSAID in which for large MLT the poleward peak should be higher than the equatorward one.

3. The double-peak PJ structure, shown in Figures 6 and 7, begins to manifest itself after 16 UT. As inferred from the behavior of geomagnetic indices (Figure 1, *a*, *b*), the greatest magnetic disturbance occurred before

10–12 UT and subsequently was insignificant up to 20 UT, when there was a brief rise in geomagnetic activity.

Thus, the polarization jet we study and DSAID presented in [He et al., 2016] have both similarities and differences. In-depth study of the double-peak PJ structures and causes of their occurrence requires further research, including small-scale structures in PJ.

## CONCLUSION

During the April 20, 2018 geomagnetic storm, using NorSat-1 satellite data at the geomagnetic latitude 40°–50° in the subauroral ionosphere we detected a polarization jet and studied its properties and characteristics. Due to the high-frequency measurements of plasma characteristics with onboard instruments, we examined the small-scale structures of the polarization jet:

- we identified temperature and electron density irregularities with spatial scales of tens to hundreds of meters;
- we showed that the electron temperature inside the polarization jet increased on average 1.5 times;
- we confirmed the previously known features of evolution of the polarization jet, such as its widening and shift toward the equator with increasing geomagnetic activity.
- we have found that as geomagnetic activity develops the electron temperature distribution in the polarization jet splits into two distinct peaks.

We thank V.L. Khalipov for the fruitful discussion of various issues related to the study of the polarization jet. We are grateful to Lasse Clausen for access to NorSat-1 satellite data [<http://tid.uio.no/plasma/norsat>]. We are also indebted to the Kyoto World Data Center for Geomagnetism [<http://wdc.kugi.kyotou.ac.jp>] and SuperMAG organizations and national agencies [<http://supermag.jhuapl.edu/info>] for data on geomagnetic activity indices.

## REFERENCES

- Anderson P.C., Heelis R.A., Hans W.B. The ionospheric signatures of rapid subauroral ion drifts. *J. Geophys. Res.* 1991, vol. 96, no. A4, pp. 5785–5792. DOI: [10.1029/90JA02651](https://doi.org/10.1029/90JA02651).
- Anderson P.C., Hanson W.B., Heelis R.A., Craven J.D., Baker D.N., Frank L.A. A proposed production model of rapid subauroral ion drifts and their relationship to substorm evolution. *J. Geophys. Res.* 1993, vol. 98, no. A4, pp. 6069–6078. DOI: [10.1029/92JA01975](https://doi.org/10.1029/92JA01975).
- Anderson P.C., Carpenter D.L., Tsuruda K., Mukai T., Rich F.J. Multisatellite observations of rapid subauroral ion drifts (SAID). *J. Geophys. Res.* 2001, vol. 106, no. A12, pp. 29585–29599. DOI: [10.1029/2001JA000128](https://doi.org/10.1029/2001JA000128).
- Benkova N.P., Kozlov E.F., Samorokin N.I., Galperin Yu.I., Beghin C. Two-dimensional snapshots of electron density in the main trough and diffuse auroral zone from a close network of ionosondes: Comparison with measurements from AUREOL-3 satellite. *The Results of the ARCAD-3 Project and of the Recent Programmes in Magnetospheric and Ionospheric Physics. Trans. of Intern. Symp. Toulouse, May 1984.* Toulouse, CNES, Cepadues-Editions, 1985, pp. 855–878.
- Bondar' E.D., Khalipov V.L., Stepanov A.E. Characteristics of a polarization jet as measured at the subauroral stations Yakutsk and Podkamennaya Tunguska. *Solnechno-zemnaya fizika* [Solar-Terrestrial Physics]. 2005, no. 8, pp. 143–144. (In Russian).
- Bryunelli B.E., Namgaladze A.A. *Fizika ionosfery* [Ionospheric Physics]. Moscow, Nauka Publ., 1988, 528 p. (In Russian).
- Burke W.J., Maynard N.C., Hagan M.P., Wolf R.A., Wilson G.R., Gentile L.C., Gussenhoven M.S., Huang C.Y., Garner T.W., Rich F.J. Electrodynamics of the inner magnetosphere observed in the dusk sector by CRRES and DMSP during the magnetic storm of June 4–6, 1991. *J. Geophys. Res.* 1998, vol. 103, iss. A12, pp. 29399–29418. DOI: [10.1029/98JA02197](https://doi.org/10.1029/98JA02197).
- Figueiredo S., Karlsson E., Marklund G. Investigation of subauroral ion drifts and related field-aligned currents and ionospheric Pedersen conductivity distribution. *Ann. Geophys.* 2004, vol. 22, pp. 923–934. DOI: [10.5194/angeo-22-923-2004](https://doi.org/10.5194/angeo-22-923-2004).
- Foster J.C., Burke W.J. SAPS: A new categorization for subauroral electric fields. *EOS Trans. AGU.* 2002, vol. 83, pp. 293–294. DOI: [10.1029/2002EO000289](https://doi.org/10.1029/2002EO000289).
- Foster J.C., Vo H.B. Average characteristics and activity dependence of the subauroral polarization stream. *J. Geophys. Res.* 2002, vol. 107, no. A12, 1475. DOI: [10.1029/2002JA009409](https://doi.org/10.1029/2002JA009409).
- Foster J.C., Park C.G., Brace L.H., Burrows J.R., Hoffman J.H., Maier E.J., Whitteker J.H. Plasmopause signatures in the ionosphere and magnetosphere. *J. Geophys. Res.* 1978, vol. 83, no. A3, pp. 1175–1182. DOI: [10.1029/JA083iA03p01175](https://doi.org/10.1029/JA083iA03p01175).
- Galperin Yu.I. Polarization jet: characteristics and a model. *Ann. Geophys.* 2002, vol. 20, no. 3, pp. 391–404. DOI: [10.5194/angeo-20-391-2002](https://doi.org/10.5194/angeo-20-391-2002).
- Galperin Yu.I., Sivtseva L.D. *Subavroral'naya verkhnyaya ionosfera* [Subauroral upper ionosphere]. Novosibirsk, Nauka Publ., 1990, 192 p. (In Russian).
- Galperin Yu.I., Ponomarev V.N., Zosimova A.G. Direct measurements of ion drift velocity in the upper ionosphere during a magnetic storm. I. Methodological issues and some measurement results in a magnetically quiet time. *Kosmicheskije issledovaniya* [Space Researches]. 1973a, vol. 11, no. 2, pp. 273–283. (In Russian).
- Galperin Yu.I., Ponomarev V.N., Zosimova A.G. Direct measurements of ion drift velocity in the upper ionosphere during a magnetic storm. II. Results of measurements during a magnetic storm on November 3, 1967. *Kosmicheskije issledovaniya* [Space Researches]. 1973b, vol. 11, no. 2, pp. 284–296. (In Russian).
- Galperin Yu.I., Ponomarev V.N., Zosimova A.G. Plasma convection in the polar ionosphere. *Ann. Geophys.* 1974, vol. 30, no. 1, pp. 1–7.
- Galperin Yu.I., Kran'ë Zh., Lisakov Yu.V., Nikolaenko L.M., Sinityn V.M., Sovo Zh.-A., Khalipov V.L. Diffuse auroral zone. I. Model of the equatorial boundary of the diffusion zones of secondary electrons in the evening and near-midnight sectors. *Kosmicheskije issledovaniya* [Cosmic Res.]. 1977, vol. 15, no. 3, pp. 421–434. (In Russian).
- He F., Zhang X.-X., Chen B. Solar cycle, seasonal, and diurnal variations of subauroral ion drifts: Statistical results. *J. Geophys. Res.: Space Phys.* 2014, vol. 119, pp. 5076–5086. DOI: [10.1002/2014JA019807](https://doi.org/10.1002/2014JA019807).
- He F., Zhang X.-X., Wang W., Chen B. Double-peak subauroral ion drifts (DSADs). *Geophys. Res. Lett.* 2016, vol. 43, pp. 5554–5562. DOI: [10.1002/2016GL069133](https://doi.org/10.1002/2016GL069133).
- Hoang H., Clausen L.B.N., Røed K., Bekkeng T.A., Trondsen E., Lybekk B., Strøm H., Bang-Hauge D.M., Pedersen A., Spicher A., Moen J.I. The Multi-Needle Langmuir Probe System on Board NorSat-1. *Space Sci. Rev.* 2018, vol. 214, iss.4, 75. DOI: [10.1007/s11214-018-0509-2](https://doi.org/10.1007/s11214-018-0509-2).
- Ievchenko I.B., Khalipov V.L., Alekseev V.N., Stepanov A.E. Dynamics of ionization of the F2 layer in the region of diffuse aurora and SAR-arc during a substorm. *Geomagnetizm i aeronomiya* [Geomagnetism and Aeronomy]. 2001, vol. 41, no. 5, pp. 642–649. (In Russian).
- Jacobsen K.S., Pedersen A., Moen J.I., Bekkeng T.A. A new Langmuir probe concept for rapid sampling of space plasma electron density. *Measurement Science and Technology.* 2010, vol. 21, iss. 8, 085902. DOI: [10.1088/0957-0233/21/8/085902](https://doi.org/10.1088/0957-0233/21/8/085902).
- Karlsson E., Marklund G., Blomberg L., Malkki A. Subauroral electric fields observed by Freja satellite: A statistical study. *J. Geophys. Res.* 1998, vol. 103, pp. 4327–4341. DOI: [10.1029/97JA00333](https://doi.org/10.1029/97JA00333).
- Khalipov V.L., Galperin Yu.I., Lisakov Yu.V., Nikolaenko L.M., Kran'ë Zh., Sinityn V.M., Sovo Zh.-A. Diffuse auroral zone. II. Formation and dynamics of the polar edge of the subauroral ionospheric trough in the evening sector. *Kosmicheskije issledovaniya* [Cosmic Res.]. 1977, vol. 15, no. 5, pp. 708–724. (In Russian).
- Khalipov V.L., Galperin Yu.I., Stepanov A.E., Bondar' E.D. Formation of polarization jet during injection of ions into the inner magnetosphere. *Adv. Space Res.* 2003, vol. 31, no. 5, pp. 1303–1308.
- Khalipov V.L., Stepanov A.E., Kotova G.A., Bondar' E.D. Position variations of the polarization jet and injection boundary of energetic ions during substorms. *Geomagnetism and Aeronomy.* 2016a, vol. 56, no. 2, pp. 174–180. DOI: [10.1134/S0016793216020080](https://doi.org/10.1134/S0016793216020080).
- Khalipov V.L., Stepanov A.E., Kotova G.A., Kobayakova S.E., Bogdanov V.V., Kaysin A.V., Panchenko V.A. Vertical plasma drift velocities in the polarization jet observation by ground Doppler measurements and driftmeters on DMSP satellites. *Geomagnetism and Aeronomy.* 2016b, vol. 56, no. 5, pp. 535–544. DOI: [10.1134/S0016793216050066](https://doi.org/10.1134/S0016793216050066).
- Kotova D.S., Zakharenkova I.E., Klimentko M.V., Ovodenko V.B., Tyutin I.V., Chuginin D.V., Chernyshov A.A., Ratovskiy K.G., Chirik N.V., Uspenskiy M.V., Klimentko V.V., Rakhmatulin R.A., Pashin A.Yu., Dmitriev A.V., Suvorova A.V. Formation of ionospheric irregularities in the East Siberian region during a geomagnetic storm on May 27–28, 2017. *Khimicheskaya fizika* [Russian Journal of Physical Chemistry B]. 2020, vol. 14, no. 2, pp. 377–389. DOI: [10.1134/S1990793120020232](https://doi.org/10.1134/S1990793120020232).
- Koustov A.V., Drayton R.A., Makarevich R.A., McWilliams K.A., St-Maurice J.-P., Kikuchi T., Frey H.U. Observations of high-velocity SAPS-like flows with the King Salmon SuperDARN radar. *Ann. Geophys.* 2006, vol. 24, pp. 1591–1608. DOI: [10.5194/angeo-24-1591-2006](https://doi.org/10.5194/angeo-24-1591-2006).
- MacDonald E.A., Donovan E., Nishimura Yu., Case N.A.,

- Gillies D.M., Gallardo-Lacourt B., Archer W.E., Spanswick E.L., Bourassa N., Connors M., Heavner M., Jackel B., Kosar B., Knudsen D.J., Ratzlaff C., Schofield I. New science in plain sight: Citizen scientist lead to the discovery of optical structure in the upper atmosphere. *Sci. Adv.* 2018, vol. 4, no. 3. DOI: [10.1126/sciadv.aaq0030](https://doi.org/10.1126/sciadv.aaq0030).
- Maynard N.C. On large poleward directed electric fields at subauroral latitudes. *Geophys. Res. Lett.* 1978, vol. 5, no. 7, pp. 617–618.
- Maynard N.C., Aggson T.L., Heppner J.P. The plasmaspheric electric field as measured by ISEE-1. *J. Geophys. Res.* 1983, vol. 88, no. A5, pp. 3981–3990.
- Mishin E.V. Interaction of substorm injections with the subauroral geospace: Multispacecraft observations of SAID. *J. Geophys. Res.* 2013, vol. 118, no. A9, pp. 5782–5796. DOI: [10.1002/jgra.50548](https://doi.org/10.1002/jgra.50548).
- Mishin E.V., Puhl-Quinn P.A., Santolik O. SAID: A turbulent plasmaspheric boundary layer. *Geophys. Res. Lett.* 2010, vol. 37, iss. 7, L07106. DOI: [10.1029/2010GL042929](https://doi.org/10.1029/2010GL042929).
- Mishin E.V., Nishimura Yu., Foster J. SAPS/SAID revisited: A causal relation to the substorm current wedge. *J. Geophys. Res.: Space Phys.* 2017, vol. 112, iss. 8, pp. 8516–8535. DOI: [10.1002/2017JA024263](https://doi.org/10.1002/2017JA024263).
- Mott-Smith H.M., Langmuir I. The theory of collectors in gaseous discharges. *Phys. Rev.* 1926, vol. 28, iss. 4, pp. 727–763. DOI: [10.1103/PhysRev.28.727](https://doi.org/10.1103/PhysRev.28.727).
- Newell P.T., Gjerloev J.W. Evaluation of SuperMAG auroral electrojet indices as indicators of substorms and auroral power. *J. Geophys. Res.* 2011, vol. 116, no. A12211. DOI: [10.1029/2011JA016779](https://doi.org/10.1029/2011JA016779).
- Nose M., Iyemori T., Sugiura M., Kamei T. Geomagnetic *Dst* index. *World Data Center for Geomagnetism, Kyoto*. 2015. DOI: [10.17593/14515-74000](https://doi.org/10.17593/14515-74000).
- Rowland D.E., Wygant J.R. Dependence of the large-scale, inner magnetospheric electric field on geomagnetic activity. *J. Geophys. Res.* 1998, vol. 103, no. A7, pp. 14959–14964.
- Seran E., Frey H.U., Fillingim H., Berthelier J.J., Pottelette R., Parks G. Demeter high resolution observations of the ionospheric thermal plasma response to magnetospheric energy input during the magnetic storm of November 2004. *Ann. Geophys.* 2008, vol. 25, iss. 12, pp. 2503–2511. DOI: [10.5194/angeo-25-2503-2007](https://doi.org/10.5194/angeo-25-2503-2007).
- Spiro R.W., Heelis R.A., Hanson W.B. Rapid subauroral ion drifts observed by Atmosphere Explorer C. *Geophys. Res. Lett.* 1979, vol. 6, iss. 8, pp. 657–660. DOI: [10.1029/GL0061008p00657](https://doi.org/10.1029/GL0061008p00657).
- Stepanov A.E., Golikov I.A., Popov V.I., Bondar' E.D., Khalipov V.L. Structural features of the subauroral ionosphere upon the occurrence of a polarization jet. *Geomagnetizm i aeronomiya* [Geomagnetism and Aeronomy]. 2011, vol. 51, no. 5, pp. 643–649. (In Russian).
- Stepanov A.E., Khalipov V.L., Golikov I.A., Bondar' E.D. *Polyarizatsionnyi dzhety: uzkie i bystrye dreifny subavroral'noi ionosfernoi plazmy* [Polarization jet: narrow and fast drifts of subauroral ionospheric plasma]. Yakutsk, 2017, 172 p. (In Russian).
- Stepanov A.E., Kobayakova S.E., Khalipov V.L. Observation of fast subauroral ionospheric plasma drifts according to the data of the Yakutsk meridional chain of stations. *Solar-Terr. Phys.* 2019a, vol. 5, no. 4, pp. 60–65. DOI: [10.12737/stp-54201908](https://doi.org/10.12737/stp-54201908).
- Stepanov A.E., Kobayakova S.E., Khalipov V.L., Kotova G.A. Results of observations of ionospheric plasma drifts in the polarization jet region. *Geomagnetism and Aeronomy*. 2019b, vol. 59, no. 5, pp. 539–542. DOI: [10.1134/S001679321905013X](https://doi.org/10.1134/S001679321905013X).
- Wang H., Lühr H., Ritter P., Kervalishvili G. Temporal and spatial effects of subauroral polarization streams on the thermospheric dynamics. *J. Geophys. Res.* 2012, vol. 117, no. A11. DOI: [10.1029/2012JA018067](https://doi.org/10.1029/2012JA018067).
- Wei D., Yu Y., Ridley A.J., Cao J., Dunlop M.W. Multi-point observations and modeling of subauroral polarization streams (SAPS) and double-peak subauroral ion drifts (DSAIDs): A case study. *Adv. Space Res.* 2019, vol. 63, pp. 3522–3535. DOI: [10.1016/j.asr.2019.02.004](https://doi.org/10.1016/j.asr.2019.02.004).
- URL: <http://tid.uio.no/plasma/norsat> (accessed May 11, 2020).
- URL: <http://wdc.kugi.kyotou.ac.jp> (accessed May 11, 2020).
- URL: <http://supermag.jhuapl.edu/info> (accessed May 11, 2020).

*How to cite this article*

Sinevich A.A., Chernyshov A.A., Chuginin D.V., Miloch W.J., Mogilevsky M.M. Studying the small-scale structure of a polarization jet during the April 20, 2018 geomagnetic storm. *Solar-Terrestrial Physics*. 2021. Vol. 7. Iss. 1. P. 17–26. DOI: [10.12737/stp-71202103](https://doi.org/10.12737/stp-71202103).